

A Dynamical Adaptive Resonance Architecture

Gregory L. Heileman, *Member, IEEE*, Michael Georgiopoulos, *Member, IEEE*, and Chaouki Abdallah, *Member, IEEE*

Abstract—A set of nonlinear differential equations that describe the dynamics of the ART1 model are presented, along with the motivation for their use. These equations are extensions of those developed by Carpenter and Grossberg [1]. It is shown how these differential equations allow the ART1 model to be realized as a collective nonlinear dynamical system. Specifically, we present an ART1-based neural network model whose description requires no external control features. That is, the dynamics of the model are completely determined by the set of coupled differential equations that comprise the model. It is shown analytically how the parameters of this model can be selected so as to guarantee a behavior equivalent to that of ART1 in both fast and slow learning scenarios. Simulations are performed in which the trajectories of node and weight activities are determined using numerical approximation techniques.

I. INTRODUCTION

THE ART1 neural network model is a self-organizing architecture capable of learning recognition categories of complex binary input patterns. The behavior of the ART1 network is effectively described in [1, sections 3–6]. Furthermore, many of the features of the ART1 model are specified via a set of nonlinear differential equations [1, section 12]. It should be noted that a number of mechanisms in the original ART1 model—such as the reset mechanism, and the resetting of node activities to zero prior to a pattern presentation—are only qualitatively described in [1]. The focus of our work is to provide a nonlinear dynamical system model that completely captures all aspects of the behavior of the ART1 network. For the sake of convenience we will refer to the dynamical system model presented here as the *augmented* ART1 network (AART1-NN), as opposed to the ART1 network (ART1-NN) presented in [1].¹

There are a number of advantages offered by the dynamical system model described here. First, it is intuitively pleasing to provide a complete mathematical description of the ART1 model. After all, this model is more than just a pattern clustering technique—it is a neural network architecture, with appropriate interconnections and describing equations, which as a whole exhibits pattern clustering capabilities. Second, the analysis of dynamical systems is a well understood and rich

area as witnessed by the recent growth in the sciences of chaos and nonlinear physics [3], [4]. A dynamical system setting, where a neural network is allowed to follow a trajectory set by the initial conditions and the external inputs, is a natural medium for studying the stability, structure, and capabilities of a network [5]. Moreover, such a setting allows us to generalize a particular network structure (e.g., the ART1 model) in order to obtain those generic properties satisfied by the network. For example, using a dynamical system setting, Kosko was able to prove the general BAM theorems [5], and we were able to use the concept of gradient systems [6] in order to generalize the structure and update rules of an on-center-off-surround network that is a simplified version of the dynamical system presented here [7]. Finally, a complete dynamical system description of the ART1 model facilitates its implementation in hardware. A circuit that implements the system of equations describing the ART1 model presented here utilizing analog electronic components has been successfully designed and verified using the PSpice circuit simulator [8], [9].

To put this dynamical system model of ART1 into perspective, it is useful to consider some related work. There has been much interest in reformulating the popular back-propagation algorithm using the dynamical system framework discussed above. For example, Pineda presented a backpropagation technique for exploiting the dynamics of a general class of neurodynamical systems [10], Williams proposed a learning algorithm for a continually running fully recurrent network [11], and Narendra and Parthasarathy discussed dynamic back-propagation as applied to recurrent networks [12]. In the area of adaptive resonance networks, the ART2 network [13]—which is used to classify analog input patterns—has been extended so as to allow a complete description of the model as a dynamical system [14].

The organization of the paper is as follows. In Section II descriptions of the architecture, network equations, and operation of the ART1 neural network (ART1-NN) are provided. This review leads to a presentation in Section III of the augmented ART1 neural network (AART1-NN). Section IV demonstrates that the AART1-NN equations exhibit a behavior identical to the ART1-NN behavior described in [1, sections 3–6]. This identical behavior is established under the assumption that the AART1-NN parameter values satisfy certain constraints. These constraints are also derived in Section IV. In Section V AART1-NN parameter values are chosen for an example network so as to satisfy the parameter constraints developed in Section IV. In Section VI we present computer simulation results that demonstrate the behavior of the AART1-NN for a number of different scenarios. Section VII summarizes our results and presents some concluding remarks.

Manuscript received September 24, 1993; revised March 5, 1993. This work was supported in part by the Boeing Computer Services under Contract W-300445, and the Florida High Technology and Industry Council.

G. L. Heileman and C. Abdallah are with the ICS Group in the Department of Electrical and Computer Engineering, University of New Mexico, Albuquerque, NM 87131 USA.

M. Georgiopoulos is with the Department of Electrical and Computer Engineering, University of Central Florida, Orlando, FL 32816 USA.

IEEE Log Number 9208989.

¹In Hirsch's classification scheme [2], the AART1-NN is classified as a dynamical system in the Cartesian product of the weight space and the node activation space. This is due to the fact that the weights in this network are adapted concurrently with the activation dynamics of the nodes.

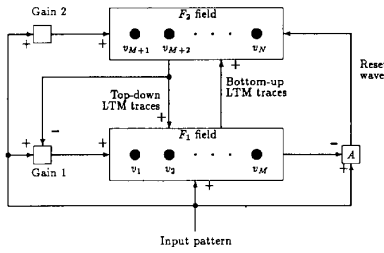


Fig. 1. The architecture of the ART1 neural network model.

II. THE ART1 NEURAL NETWORK

In the following sections we briefly summarize the ART1-NN architecture, operation, and equations that describe the network dynamics. A more complete description of the ART1 model is given in [1], and a number of useful results and theorems regarding the capabilities of this model are given in [1], [15], [16].

A. Architecture

The major components of the ART1 model are depicted in Fig. 1. These components can be grouped into two subsystems—the attentional and orienting subsystems. The F_1 and F_2 fields in the attentional subsystem each consist of a single layer of nodes. These nodes are used to encode patterns of short term memory (STM) activity, while the weighted connections between the nodes in the F_1 and F_2 fields are used to store long term memory (LTM) traces. Each node in the F_1 field is connected via bottom-up connections to all nodes in the F_2 field, and each node in the F_2 field is connected via top-down connections to each of the F_1 field nodes. In addition, the set of nodes comprising the F_2 field are completely connected.

The orienting subsystem, A , receives input from the F_1 field nodes, as well as from the input pattern. The orienting subsystem will generate a reset wave to the F_2 field whenever the input pattern is not matched close enough to the pattern of STM activity across the F_1 field.

B. Operation

The operation of the ART1-NN can be described as follows. STM activity is induced in the F_1 field by the introduction of an input pattern. The components of the input pattern comprise the bottom-up input to the F_1 field. A node with activity below or above its threshold is said to be *subliminally* or *supraliminally* active, respectively. The threshold is typically a small positive constant. A node is said to be *activated* if its activity increases from a level below its threshold to a level above its quenching threshold. In addition, a node is said to be *deactivated* if its activity drops from a level above its threshold to a level below its threshold. The orienting subsystem, A , is nonspecifically activated by the input pattern. The STM activity across the F_1 field generates an output from the F_1 field that inhibits A . This output activity is multiplied by the bottom-up LTM traces, and the result is a bottom-up input which is supplied to the F_2 field. Next, a contrast enhancement process (competition cycle) occurs among the

F_2 field nodes, generating a STM activity across the F_2 field. A special case of this contrast enhancement mechanism is one in which only one node is chosen to remain supraliminally active in the F_2 field. This form of contrast enhancement, often referred to as a *gated dipole field*, is assumed throughout this paper. The output activity of the F_2 field is transformed through a multiplication process with the top-down LTM traces to generate a top-down input to the F_1 field. At this point, new STM activity is generated across the F_1 field. If there is significant mismatch between bottom-up and top-down inputs at the F_1 field, this new STM activity results in a new output activity from the F_1 field which causes a decrease in the total inhibition impinging upon A from the F_1 field. As a result, the input-driven activation of A may release a nonspecific reset wave which inhibits the STM activity at the F_2 field. This inhibition leads to the elimination of the top-down input affecting the activity of the F_1 field nodes. Hence, the initial STM activity is reinstated across the F_1 field. Once again, this STM activity across the F_1 field generates an output from the F_1 field which produces the same bottom-up input at the F_2 field as before. Since the node initially chosen in the F_2 field remains inhibited, a new node in the F_2 field can now be chosen. If once more the new top-down input significantly mismatches the bottom-up input at the F_1 field, then the search for an appropriate F_2 field node continues until a node is found that does not lead to a reset, or until all nodes in the F_2 field are found inappropriate to code (i.e., learn) the input pattern. If a reset wave is not generated by the orienting system after the activation of an F_2 field node, then this node is said to *code* the input pattern.

C. Network Equations

The operation of the ART1 network discussed above can be represented by a set of nonlinear differential equations. The activity of the network nodes is described by the following differential equation:

$$\epsilon \frac{d}{dt} x = -x + (1 - Ax)J^+ - (B + Cx)J^- \quad (1)$$

where x is the nodal activity; while J^+ and J^- , which represent the total excitatory and inhibitory input to the node, respectively, are functions of x . Equation (1) is called a *shunting* differential equation because J^+ and J^- multiply the node activity x . Note that if $A > 0$ and $C > 0$, then the activity of the node remains in the bounded range $[-BC^{-1}, A^{-1}]$ no matter how large J^+ and J^- become, assuming the node activity is initially in this range. Also notice that the activity of the node decays to a resting level of 0 when $J^+ = J^- = 0$.

We denote nodes in the F_1 field by v_i and nodes in the F_2 field by v_j . The index of the nodes in the F_1 field ranges from 1 to M , while the index of the nodes in the F_2 field ranges from $M + 1$ to N . We also denote the activity of a node v_i by x_i , and the activity of a node v_j by x_j . In particular, the activity of a node v_i in the F_1 field satisfies the following differential equation

$$\epsilon_1 \frac{d}{dt} x_i = -x_i + (1 - A_1 x_i)J_i^+ - (B_1 + C_1 x_i)J_i^- \quad (2)$$

The total excitatory input to node v_i is given by

$$J_i^+ = I_i + D_1 \sum_j f_2(x_j) z_{ji} \quad (3)$$

where D_1 is a constant, I_i is the component of the binary input pattern I that is received by node v_i , $f_2(x_j)$ is the output activity generated by node v_j with activity x_j , and z_{ji} is the value of the top-down LTM trace corresponding to the connection between node v_j in the F_2 field and node v_i in the F_1 field. In (3), and throughout this paper, we will assume that the output activity generated by a node v_j with activity x_j is the threshold function

$$f_2(x_j) = \begin{cases} 1, & \text{if } x_j > \delta_2; \\ 0, & \text{otherwise} \end{cases} \quad (4)$$

where δ_2 is the threshold of every node v_j in the F_2 field. The total inhibitory input to node v_i is given by

$$J_i^- = \sum_j f_2(x_j). \quad (5)$$

The activity of a node v_j in the F_2 field satisfies the following differential equation

$$\epsilon_2 \frac{d}{dt} x_j = -x_j + (1 - A_2 x_j) J_j^+ - (B_2 + C_2 x_j) J_j^-. \quad (6)$$

The total excitatory input to node v_j is calculated as

$$J_j^+ = f_2(x_j) + T_j \quad (7)$$

with

$$T_j = D_2 \sum_i f_1(x_i) z_{ij} \quad (8)$$

where D_2 is a constant. In (8), and throughout this paper, we will assume that the output activity generated by a node v_i with activity x_i is the threshold function

$$f_1(x_i) = \begin{cases} 1, & \text{if } x_i > \delta_1; \\ 0, & \text{otherwise} \end{cases} \quad (9)$$

where δ_1 is the threshold of every node v_i in the F_1 field. Finally, the total inhibitory input to a node v_j in the F_2 field is given by

$$J_j^- = \sum_{k \neq j} f_2(x_k). \quad (10)$$

The value of the bottom-up LTM trace, z_{ij} , associated with an arc connecting node v_i in the F_1 field to node v_j in the F_2 field is determined by the following differential equation

$$\epsilon_z \frac{d}{dt} z_{ij} = K_1 f_2(x_j) [-E_{ij} z_{ij} + f_1(x_i)]. \quad (11)$$

In the present model, K_1 is a constant and E_{ij} is given by

$$E_{ij} = f_1(x_i) + L^{-1} \sum_{k \neq i} f_1(x_k) \quad (12)$$

where L is a constant > 1 . Combining (11) and (12) yields

$$\epsilon_z \frac{d}{dt} z_{ij} = -K \left[(L-1) f_1(x_i) + \sum_k f_1(x_k) \right] \cdot f_2(x_j) z_{ij} + KL f_1(x_i) f_2(x_j) \quad (13)$$

with $K = K_1 L^{-1}$.

The value of the top-down LTM trace, z_{ji} , associated with an arc connecting node v_j in the F_2 field to node v_i in the F_1 field is determined by the following differential equation:

$$\epsilon_z \frac{d}{dt} z_{ji} = -K_2 E_{ji} f_2(x_j) z_{ji} + K_2 f_1(x_i) f_2(x_j). \quad (14)$$

The present model assumes that

$$K_2 = E_{ji} = 1. \quad (15)$$

The parameters ϵ_1, ϵ_2 , and ϵ_z that appear in the previous equations are referred to as *learning rates*. These values determine the rate of change of the variables (STM activity in the F_1 field, STM activity in the F_2 field, and bottom-up or top-down LTM traces between pairs of nodes in the F_1 and F_2 fields) that are characterized by the above equations. A smaller value for the parameter ϵ results in a faster rate of change of the variable described by the differential equation under consideration. For example, if $\epsilon_1, \epsilon_2 \ll \epsilon_z$, then the rate of change of the STM activity in the F_1 and F_2 fields is much faster than the rate of change of the bottom-up and top-down LTM traces between pairs of nodes in the F_1 and F_2 fields.

III. THE AUGMENTED ART1 NEURAL NETWORK

A number of implementation issues that are not directly addressed in the ART1 model [1] are considered here. These include:

- i) The manner in which the mismatch-mediated reset wave can be generated.
- ii) The approach taken to ensure that an F_2 field node remains inactive, once it is reset, until a new input pattern is presented.
- iii) A way of automatically driving the activity of every node in the network to its resting value of zero whenever an input pattern is removed from the network.

Below we address each of these issues separately. The approach taken to resolve the aforementioned issues is directed towards a solution that will facilitate a dynamical system realization of the ART1-NN. The resolution of these issues will involve the addition of nodes in the ART1-NN architecture, and minor modifications to the original ART1 neural network equations presented in Section II-C. The resulting model is termed the AART1-NN. The major components of the AART1-NN are shown in Fig. 2. It is instructive to compare the ART1-NN architecture of Fig. 2 to the AART1-NN architecture depicted in Fig. 1. One immediate observation is that the F_2 field nodes in the ART1-NN correspond to the first layer of nodes in the F_2 field of the AART1-NN architecture. That is, the first layer of nodes in the F_2 field of the AART1-NN is used for category representation, as is the F_2 field in the ART1-NN.

Resolution of Issue i: Let $|I|$ denote the number of input pathways which receive positive input when the input pattern I is presented. Also, let $|X|$ denote the number of nodes in the F_1 field that are supraliminally active during the presentation of the input pattern I . In the ART1 model, each of the $|I|$ input pathways sends an excitatory signal of fixed size P to

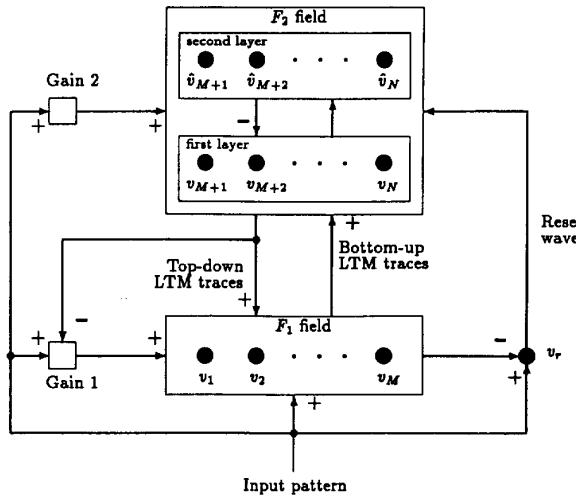


Fig. 2. The architecture of the augmented ART1 neural network model.

the orienting subsystem A , and each of the $|X|$ supraliminally active nodes in the F_1 field generates an inhibitory signal of fixed size Q that also impinges on the orienting subsystem. Furthermore, the orienting subsystem in the ART1 model generates a nonspecific reset wave whenever

$$P|I| > Q|X| \quad (16)$$

or equivalently, whenever

$$\frac{|X|}{|I|} < \rho = \frac{P}{Q} \quad (17)$$

where ρ , the *vigilance parameter*, is chosen in the interval $(0, 1]$.

The generation of the reset wave by the orienting subsystem can be accomplished within the framework of a dynamical system model through the introduction of a *reset node*, v_r , whose activity satisfies the following differential equation:

$$\epsilon_r \frac{d}{dt} x_r = -A_r x_r + U \left[P \sum_{i=1}^M I_i - Q \sum_{i=1}^M f_1(x_i) \right] \quad (18)$$

where U is the unit step function

$$U(x) = \begin{cases} 1, & \text{if } x > 0; \\ 0 & \text{otherwise.} \end{cases} \quad (19)$$

Note that the activity of the reset node becomes positive whenever $\frac{|X|}{|I|} < \rho$, and decays exponentially to zero whenever $\frac{|X|}{|I|} \geq \rho$. The output activity of the reset node, $f_r(x_r)$, which corresponds to the nonspecific reset wave, satisfies

$$f_r(x_r) = \begin{cases} 1, & \text{if } x_r > \delta_r; \\ 0, & \text{otherwise.} \end{cases} \quad (20)$$

The introduction of a reset node whose activity satisfies (18), and whose output activity is determined by (20), provides a mechanism for the generation of the reset wave by the orienting subsystem, as required by the ART1 model, whenever there is a sufficient mismatch between the input pattern I and the activity pattern X across the F_1 field.

Resolution of Issue ii: An important property of the ART1 model is that the reset wave selectively and enduringly inhibits active F_2 field nodes until the input pattern is removed. This can be accomplished within the framework of a dynamical system realization of ART1 by augmenting the F_2 field with a set of inhibitory nodes (second layer of the F_2 field in Fig. 2), whose sole purpose is to implement the selective and enduring inhibition of the reset mechanism. In this case, every node v_j in the F_2 field is assigned an inhibitory node \hat{v}_j whose activity, \hat{x}_j , satisfies the following differential equation

$$\epsilon_2 \frac{d}{dt} \hat{x}_j = -[1 - g(I)]\hat{x}_j + g(I)f_r(x_r)f_2(x_j) \quad (21)$$

where

$$g(I) = \begin{cases} 1, & \text{if } \sum_{i=1}^M I_i \neq 0; \\ 0, & \text{otherwise.} \end{cases} \quad (22)$$

As can be seen from the above equations, the activity of an F_2 field inhibitory node can only become positive when the following actions are satisfied simultaneously: a nonzero input pattern is being presented to the network, a reset wave is being emitted by the reset node, and the corresponding node in the F_2 field is supraliminally active. Once the activity of an F_2 field inhibitory node has become positive, its activity decays exponentially to zero only when the input pattern is removed. In conjunction with a modification to the differential equation characterizing the activity of the first layer of F_2 field nodes, this mechanism will allow the implementation of the selective and enduring inhibition required after a reset event, and as long as the input pattern is present. Specifically, the total inhibitory input to node v_j in the F_2 field, (10), is modified as

$$J_j^- = \sum_{k \neq j} f_2(x_k) + \hat{f}_2(\hat{x}_j) \quad (23)$$

where $\hat{f}_2(\hat{x}_j)$ is the output of the F_2 field inhibitory node \hat{v}_j . This modification causes the total inhibitory input to v_j to remain positive as long as $\hat{f}_2(\hat{x}_j)$ is positive. The output of an F_2 field inhibitory node obeys the equation:

$$\hat{f}_2(\hat{x}_j) = \begin{cases} 1, & \text{if } \hat{x}_j > \hat{\delta}_2; \\ 0, & \text{otherwise.} \end{cases} \quad (24)$$

These modifications and additions to the original ART1-NN equations allow the F_2 field of the AART1-NN to behave as a gated dipole field within the dynamical systems framework.

Resolution of Issue iii: A modification to the equation describing the total excitatory input to an F_2 field node must also be made to allow the ART1 implementation to operate as a true dynamical system. The aforementioned modification will allow the activity of the F_1 and F_2 field nodes, as well as the activity of the reset node to be reset to zero whenever an input pattern is removed from the network. This can be accomplished in the following manner. When an input pattern is removed from the network, it should be followed by the presentation of the zero pattern. This will rapidly drive the activity of nodes in the F_1 and F_2 field to zero if we modify (7) as

$$J_j^+ = f_2(x_j)g(I) + D_2 \sum_i f_1(x_i)z_{ij}. \quad (25)$$

TABLE II
TIME INSTANCES PERTAINING TO THE OPERATION OF THE
AART1-NN. THE SUPERSCRIPIT ASSOCIATED WITH A SPECIFIC TIME
INSTANCE REPRESENTS THE NUMBER OF NODES IN THE FIRST LAYER
OF THE F_2 FIELD THAT HAVE BEEN SEQUENTIALLY ACTIVATED
DURING THE PRESENTATION OF THE CURRENT INPUT PATTERN

Time Instance	Interpretation
t_0	All nodes are subliminally active, and a nonzero input pattern I is presented at the F_1 field.
$t_1^{\gamma-1}$	The output pattern at the F_1 field is equal to I .
t_2^1	A single node, v_{M+1} , in the first layer of the F_2 field becomes supraliminally active.
t_3^1	The reset node v_r becomes supraliminally active.
t_4^2	Node v_{M+1} in the first layer of the F_2 field becomes subliminally active.
t_5	The input pattern I is withdrawn from the F_1 field.

layer of the F_2 field. Thus, the superscript of a time instance defined in Table II corresponds to the number of nodes in the first layer of the F_2 field of the AART1-NN that have been sequentially activated during the presentation of input pattern I .

Because the time instances defined in Table II are equivalent to those defined in Table I, it follows that the behavior of the AART1-NN will be identical to that of the ART1-NN if it can be shown that the AART1-NN operates in a manner similar to Statement 1. Specifically, consider a nonzero input pattern I belonging to the class of patterns described as Case 1 or Case 2 above. If I is presented to the F_1 field of an AART1-NN, then the behavior of this network will be equivalent to that of an ART1-NN if the following statement holds:

Statement 2: During the presentation of the nonzero input pattern I to the F_1 field of the AART1-NN, the following time instances can be identified in order of occurrence:

Case 1: $t_0, t_1^0, t_2^1, t_3^1, t_4^1, t_1^1, t_2^2, t_3^2, t_4^2, \dots, t_1^{\gamma-3}, t_2^{\gamma-2}, t_3^{\gamma-2}, t_4^{\gamma-2}, t_1^{\gamma-2}, t_2^{\gamma-1}, t_3^{\gamma-1}, t_4^{\gamma-1}, t_1^{\gamma-1}, t_2^{\gamma}, t_3^{\gamma}, t_4^{\gamma}$.

Case 2: $t_0, t_1^0, t_2^1, t_3^1, t_4^1, t_1^1, t_2^2, t_3^2, t_4^2, \dots, t_1^{\gamma-3}, t_2^{\gamma-2}, t_3^{\gamma-2}, t_4^{\gamma-2}, t_1^{\gamma-2}, t_2^{\gamma-1}, t_3^{\gamma-1}, t_4^{\gamma-1}, t_1^{\gamma-1}, t_2^{\gamma}, t_3^{\gamma}, t_4^{\gamma}, t_5$.

In this case, the first competition cycle starts at time t_1^0 and ends at time t_2^1 , while the γ -th competition cycle ($\gamma \geq 2$) starts at time $t_4^{\gamma-1}$ and ends at time t_5^{γ} . The fast and slow learning operations of the AART1-NN are defined in the same manner as they were for the ART1-NN.

In the next section we prove that under certain AART1-NN parameter constraints, the AART1-NN behaves according to Statement 2. Consequently, we prove that under these parameter constraints, the behavior of the AART1-NN is identical to that of the ART1-NN. In the proof of Statement 2 we will assume, without loss of generality, that a nonzero input pattern I belonging to the class of patterns described as Case 1 above is presented to the AART1-NN. We will then prove that during the presentation of this pattern, the time instances included in Statement 2 under Case 1 can be identified. The proof of Statement 2 is accomplished by demonstrating that with the appropriate parameter values, each time instance occurs in the order given. That is, we will show that if we start with time instance t_0 , the next identifiable time instance is t_1^0 , and if we start with time instance t_1^0 the next identifiable time instance is t_2^1 , etc., until time instance t_5 is reached.

It should be emphasized that Statement 2 describes the behavior of the AART1-NN only when a nonzero input pattern is presented at its F_1 field. The operation of the AART1-NN during the presentation of the zero pattern is easily determined from the AART1-NN equations. It can be shown that the presentation of the zero pattern to the F_1 field of the AART1-NN drives the activities of all the nodes in the network to zero. Since the zero pattern is always presented between the presentation of any two nonzero patterns, it follows that the AART1-NN equations satisfy a key ART1-NN design constraint, namely:

- **ART1 design constraint #1:** The activities of all the network nodes in the ART1-NN should be reset to zero prior to the presentation of any nonzero input pattern at its F_1 field.

During the proof of Statement 2, the AART1-NN parameter values will be chosen so as to satisfy a number of additional ART1 design constraints given below:

- **ART1 design constraint #2:** The input pattern I must be able to instate itself across the F_1 field without triggering a reset event, at least until an F_2 field node becomes active and sends top-down signals to the F_1 field.
- **ART1 design constraint #3:** The order of the O_j 's (i.e., the bottom-up inputs to the F_2 field) determine the order of search in the F_2 field, no matter how many times the F_2 field is reset.
- **ART1 design constraint #4:** During the presentation of the input pattern I at the F_1 field, a node in the F_2 field that wins a competition cycle can only be reset if there is sufficient mismatch between bottom-up and top-down inputs.

ART1 design constraint #1 is explicitly stated in [1], while ART1 design constraint #2 is explicitly stated in [17] as one of the fundamental ART design constraints. Finally, ART1 design constraints #3 and #4 are stated in [1] as Theorem 3 and Corollary 1, respectively.

B. Proof of Statement 2

In this section we prove Statement 2. To facilitate this proof we present in Appendix A a set of key AART1-NN equations. Before we proceed with the proof, let us first refer to a number of constraints that are important for the successful operation of the ART1-NN, and as a result for the successful operation of the AART1-NN. These are constraints CON1–CON7 included in Table III.

CON1 requires the STM values in the AART1-NN to change at a much faster rate than the LTM values. Furthermore, the requirement $\epsilon_r \ll \epsilon_z$ implies that the reset node in the AART1-NN responds very quickly (compared to the LTM changes in the network) to mismatches between bottom-up and top-down inputs at the F_1 field of the AART1-NN. CON1 guarantees that no significant LTM learning occurs in the AART1-NN unless the node picked in the F_2 field of the AART1-NN is the node that codes the input pattern. An immediate implication of CON1 is that it allows us to assume that the LTM traces in the AART1-NN stay constant from the time that the input pattern is presented, until the time that

TABLE III
CONSTRAINTS FOR SUCCESSFUL OPERATION OF THE AART1-NN

CON1	$\epsilon_1, \epsilon_2, \epsilon_r \ll \epsilon_s$
CON2	$A_1 > 0, C_1 > 0, A_2 > 0, C_2 > 0$
CON3	$B_1 > 0, D_1 > 0, B_2 > 0, D_2 > 0$
CON4	$0 < \rho < 1$
CON5	$L > 1, 0 < z_{ij}(0) < L(L-1+M)^{-1}$
CON6	$[B_1 - 1 + \delta_1(1+A_1+C_1)] [D_1(1-\delta_1 A_1)]^{-1} < z_{ij}(0) \leq 1$
CON7a	$\max(1, D_1) - \delta_1(1+A_1+C_1) < B_1$
CON7b	$B_1 < 1 + D_1 - \delta_1(1+A_1+D_1 A_1 + C_1)$
CON8	$\delta_r > A_1^{-1} \{1 - [1 - \delta_1(1+A_1)]^{(1+\rho)^{-1}}\}$
CON9	$B_2 > O_{\max}$
CON10	$B_2 > 1 + O_{\max}$
CON11a	$C_2 > 1 + A_2 O_{\max}$
CON11b	$B_2 = p_1 O_{\max}^2, C_2 = p_1 O_{\max}$
CON11c	$B_2 C_2^{-1} > \delta_2$
CON11d	$p_1^2 \ll 1$
CON12	$p_1 \approx \delta_1$
CON13	$\epsilon_1 \leq 0.1 \epsilon_2, A_2 O_{\max} < A_1$
CON14	$O_{M+1} < p_1 O_{M+1}$
CON15	$-p_2 O_{\max} p_2 + (1-p_2) O_{\max}(1+A_2 O_{\max})^{-1} < \delta_2$
CON16	$(1+A_1)^{-1} > \delta_1$
CON17	$A_1^{-1} > \delta_r$

the node in the first layer of its F_2 field that codes the input pattern is chosen. CON2 guarantees that the activity x_i will be constrained in the interval $[-B_1 C_1^{-1}, A_1^{-1}]$, and that the activity x_j will be constrained in the interval $[-B_2 C_2^{-1}, A_2^{-1}]$. CON3, and the fact that the z_{ij} 's and z_{ji} 's are nonnegative (see constraints CON5, CON6, CON7, and (13) and (14)), ensures that J_i^+ and J_j^+ are indeed excitatory signals, and that J_i^- and J_j^- are indeed inhibitory signals. CON4 is required for the successful operation of the reset mechanism. CON5 is important for the satisfaction of the direct access inequality—for more details see [1]. CON6 and CON7 are necessary for the validity of the $\frac{2}{3}$ rule (see equation (A.2) in Appendix A).

We now proceed with the proof of Statement 2. Consider a nonzero input pattern I which is presented to the F_1 field of the AART1-NN, and assume without loss of generality that this pattern belongs to the class of patterns previously described as Case 1. We will prove that under certain AART1-NN parameter constraints, the time instances included in Statement 2 under Case 1 can be identified. This validates Statement 2 for Case 1, and obviously for Case 2 as well.

The Time Interval After t_0 : We begin by assuming that a nonzero input pattern I is presented to the F_1 field of the AART1-NN at time instance t_0 . The activities of all the nodes in the F_1 field are equal to zero at t_0 . It is easy to see that we can identify a time, after t_0 , at which the output pattern at the F_1 field is equal to I . We have already denoted the earliest such time instance as t_1^0 . During the time interval $(t_0, t_1^0]$ the activity of every node at the F_2 field is equal to zero. Furthermore, during the time interval (t_0, t_1^0) , there is mismatch at the F_1 field. This is due to the fact that the pattern I has not yet been instated across the F_1 field. The parameters of the AART1-NN must be chosen so as to satisfy ART1 design constraint #2. To satisfy this constraint it suffices to choose the AART1-NN parameters so that the reset node is subliminally active at time instance t_1^0 . In Appendix B we show that by choosing the AART1-NN parameters according to CON8 in Table III, we ensure that the reset node v_r is subliminally active at time instance t_1^0 .

The Time Interval After t_1^0 : At time instance t_1^0 a node v_j in the F_2 field receives bottom-up input O_j from the F_1 field,

and satisfies equation (A.3) after time instance t_1^0 . In (A.3), t_a corresponds to t_1^0 and T_j corresponds to O_j . Since every node in the first layer of the F_2 field has an activity of zero at t_1^0 , and $T_j = O_j$, we can identify a time, after t_1^0 , at which the only node in the first layer of the F_2 field that is supraliminally active is v_{M+1} —we have already denoted this time instance as t_2^1 . As a result, ART1 design constraint #3 is satisfied in the first competition cycle (i.e., in the interval $(t_1^0, t_2^1]$). In the time interval $(t_1^0, t_2^1]$ the reset node satisfies equation (A.7) with $t_a = t_1^0$. Note that by choosing the AART1-NN parameters according to CON8 we guarantee that $x_r(t_1^0) < \delta_r$. Hence, at t_2^1 the reset node v_r is still subliminally active. Thus, ART1 design constraint #4 is also valid in the first competition cycle. Note that at time t_2^1 there is no mismatch between bottom-up and top-down inputs at the F_1 field.

The Time Interval After t_2^1 : After time instance t_2^1 every node v_j ($j \neq M+1$) satisfies equation (A.4) with $t_a = t_2^1$. Note that $x_j(t_2^1) < \delta_2$ for $j \neq M+1$. Let us choose the parameter B_2 according to CON9 of Table III, where O_{\max} is an upper bound on the O_j 's for any input pattern presented to the AART1-NN. Choosing B_2 according to constraint CON9 guarantees that no other node in the first layer of the F_2 field becomes supraliminally active as long as v_{M+1} is supraliminally active. In the time interval after t_2^1 , certain nodes in the F_1 field receive bottom-up, as well as top-down input. An arbitrary node v_i in the F_1 field that receives bottom-up and weak top-down input will become subliminally active some time after t_2^1 . Let us assume, without loss of generality, that enough nodes in the F_1 field receive bottom-up and weak top-down input so as to cause a positive input to the reset node. Once these nodes become subliminally active, the activity of the reset node will satisfy (A.6), and the reset node will generate a reset wave at some time after t_2^1 . We have previously denoted this time instance as t_3^1 .

The Time Interval After t_3^1 : The reset wave initiated at time instance t_3^1 will cause an excitatory input to be supplied to the inhibitory node \hat{v}_{M+1} . This results in the activation of \hat{v}_{M+1} , which in turn produces an inhibitory input to node v_{M+1} . From this time instance, node v_{M+1} in the F_2 field will satisfy (A.5). Let us choose parameter B_2 according to CON10 of Table III. The satisfaction of CON10 guarantees that the supraliminally active node v_{M+1} will become subliminally active at some time after t_3^1 . We have previously denoted this time instance as t_4^1 .

The Time Interval After t_4^1 : At time instance t_4^1 , the previously supraliminally active node v_{M+1} is subliminally active, and it will stay subliminally active as long as the input pattern is present. The deactivation of node v_{M+1} signals the beginning of the second competition cycle. Once v_{M+1} becomes subliminally active, the activities of all subliminally active nodes in the F_1 field that receive bottom-up input will start to increase. The output activity at the F_1 field is now changing from $X \subset I$ to $X = I$. The satisfaction of ART1 design constraint #3 during the second competition cycle is not a trivial matter—as it was when we were examining the first competition cycle. This is because the competition cycle starts at time instance t_4^1 , and from t_4^1 until the time that the output activity across the F_1 field becomes equal to I , the bottom-up

inputs T_{M+2} and T_j ($j \neq M+1, M+2$) can be different from the bottom-up inputs O_{M+2} and O_j ($j \neq M+1, M+2$) that should determine the order of search in the AART1-NN. To make this point clearer, we present in Appendix C an extreme case where $T_{M+2} = 0$ and $T_{M+3} = O_{M+3}$. To ensure that the AART1-NN does not perform the search in an erroneous order (e.g., a search of node v_{M+3} prior to the search of node v_{M+2} for the example in Appendix C) we require that the output activity across the F_1 field be restored to I long before the second competition cycle ends. Thus, the AART1-NN will have sufficient time to overcome the detrimental effects of a situation where $T_{M+2} < T_j$ ($j \neq M+1, M+2$) at the beginning of the second competition cycle. We denote this requirement as Requirement A. Below we develop a set of AART1-NN parameter constraints for satisfying Requirement A.

Let us assume that Requirement A is true. We will now prove that this assumption is valid under certain AART1-NN parameter constraints. Consider a node v_i that receives a bottom-up input from the input pattern I , and is subliminally active at time instance t_4^1 . After t_4^1 the activity of this node satisfies (A.1) with $t_a = t_4^1$ and $x_i(t_4^1) < \delta_1$. If we assume that among the nodes in the F_1 field that are subliminally active at t_4^1 , node v_1 becomes supraliminally active last, we can write

$$t_1^1 - t_4^1 = \ln \left[\frac{x_1(t_4^1)(1 + A_1) - 1}{\delta_1(1 + A_1) - 1} \right] (1 + A_1)^{-1} \epsilon_1. \quad (26)$$

In (26), t_1^1 denotes the time that the output activity across the F_1 field is equal to I . Consider now a node v_j ($j \neq M+1$) at time instance t_4^1 . Let us denote by $x_j^u(t)$ an upper bound for the activity of node v_j , for t in the time interval $(t_4^1, t_1^1]$. Note that $x_j^u(t)$ satisfies (A.3) with $t_a = t_4^1$, $x_j^u(t_4^1) = x_j(t_4^1) < \delta_2$, and $T_j = O_j$. The reason that $x_j^u(t)$ is an upper bound on $x_j(t)$ for $t \in (t_4^1, t_1^1]$ is because in this time interval, the bottom-up input T_j to node v_j increases towards its maximum value of O_j , and O_j is attained at time instance t_1^1 . It is obvious that our assumption regarding the validity of Requirement A will be true if the quantity $\delta_2 - x_j^u(t_1^1)$ ($j \neq M+1$) is positive, and in fact as large as possible. The quantity $x_j^u(t_1^1)$ is given by (see (26) and (A.3)):

$$x_j^u(t_1^1) = x_j(t_4^1) \Psi_1 \frac{(1 + A_2 O_j) \epsilon_1}{(1 + A_1) \epsilon_2} + \frac{O_j}{1 + A_2 O_j} \times \left\{ 1 - \Psi_1 \frac{(1 + A_2 O_j) \epsilon_1}{(1 + A_1) \epsilon_2} \right\} \quad (27)$$

with

$$\Psi_1 = \frac{1 - \delta_1(1 + A_1)}{1 - x_1(t_4^1)(1 + A_1)}. \quad (28)$$

One way of making the quantity $\delta_2 - x_j^u(t_1^1)$ as large as possible is to force $x_j^u(t_1^1)$ to be as small as possible. Thus, we choose the AART1-NN parameters so that the value of $x_j(t_4^1)$ is approximately equal to its minimum value of $-B_2 C_2^{-1}$. In Appendix D we show that this can be achieved by choosing the AART1-NN parameter values according to CON11 in Table III. Since CON11 guarantees that $x_j(t_4^1)$ is negative, we can now choose the AART1-NN parameters as in CON12 and CON13. CON12 guarantees that the value of

Ψ_1 is close to one (note that $x_1(t_4^1)$ is lower bounded by p_4 and upper bounded by δ_1), while CON13 guarantees that the exponent of Ψ_1 is small. Constraint CON11, which implies $x_j(t_4^1) \approx -B_2 C_2^{-1} = -O_{\max}$ (this is proven in Appendix D), in conjunction with CON12 and CON13 prove the validity of Requirement A.

At time instance t_1^1 , the output activity across the F_1 field is equal to I . The AART1-NN must satisfy ART1 design constraint #3 in the second competition cycle that started at time instance t_4^1 . The implication of ART1 design constraint #3 in this competition cycle is that node v_{M+2} will be the first node activated after time instance t_1^1 . In Appendix E we show that under constraint CON14 of Table III, ART1 design constraint #3 is satisfied in the second competition cycle. The time of activation of node v_{M+2} was previously denoted by time instance t_2^2 . The index n in CON14 corresponds to the index of the competition cycle under consideration. For example, since we are now interested in the second competition cycle, $n = 2$. It is worth noting from Table III that $p_5 \approx 1$ (due to CON12 and CON13), and as a result $p_7 \approx 1$. This implies that CON14 does not actually impose hard constraints on the O_j values. It is also worth noting that we do not have complete control over the O_j values—they depend, among other things, on the set of input patterns. The reason that ART1 design constraint #3 is satisfied under the mild conditions on the O_j 's imposed by CON14 is because we previously guaranteed the satisfaction of Requirement A.

We must also satisfy ART1 design constraint #4 during the second competition cycle. The satisfaction of this design constraint in the second competition cycle requires that the reset node be subliminally active at time t_2^2 . This is due to the fact that at time t_2^2 , there is no mismatch between bottom-up and top-down inputs at the F_1 field. We know that the reset node in the AART1-NN is supraliminally active at time instance t_4^1 . We also know that it might be subliminally active at time instance t_1^1 . If the reset node is subliminally active at time t_1^1 , then we immediately satisfy ART1 design constraint #4 in the second competition cycle, because we know that the reset node will be subliminally active at time t_2^2 as well. If on the contrary, the reset node is supraliminally active at time instance t_1^1 , we need to guarantee that it will become subliminally active by time t_2^2 . In Appendix F we show that this is indeed true under constraint CON15 of Table III. Hence, we can state that ART1 design constraint #4 is valid in the second competition cycle provided that CON15 is satisfied.

The Time Intervals After t_2^2 , $2 \leq \gamma \leq \Gamma - 1$: For every γ such that $2 \leq \gamma \leq \Gamma - 1$ we can show that t_3^γ is the next identifiable time instance after time instance t_2^γ . The approach is similar to the one followed after time interval t_1^1 .

The Time Intervals After t_3^γ , $2 \leq \gamma \leq \Gamma - 1$: For every γ such that $2 \leq \gamma \leq \Gamma - 1$ we can show that t_4^γ is the next identifiable time instance after time instance t_3^γ . The approach is similar to the one followed after time interval t_1^1 .

The Time Intervals After t_4^γ , $2 \leq \gamma \leq \Gamma - 1$: For every γ such that $2 \leq \gamma \leq \Gamma - 1$ we can show that t_1^γ is the next identifiable time instance after time instance t_4^γ , and we can also show that $t_2^{\gamma+1}$ is the next identifiable time instance after time instance t_1^γ . The approach is similar to the one followed

after time interval t_4^1 . The only difference now is that we are dealing with different competition cycles (i.e., competition cycles $3, 4, \dots, \Gamma$).

Thus, after time t_2^2 , time instances occur in the order prescribed by Statement 2 under Case 1, and no additional AART1-NN parameter constraints are necessary beyond those already developed (i.e., CON1–CON15). It is worth pointing out that CON14 depends on the index n of the competition cycle under consideration. For Case 1, which is under investigation, the range of n is over the set $\{2, 3, \dots, \Gamma\}$. For Case 2 though, the range of n is over the set $\{2, 3, \dots, N - M - 1\}$. Since our objective is to guarantee the validity of Statement 2 under both cases, we take the range of n to be the set $\{2, 3, \dots, N - M - 1\}$.

The Time Interval After t_2^Γ : At time instance t_2^Γ the Γ -th node in the first layer of the F_2 field has been activated, and this node codes the input pattern I (Case 1). LTM learning takes place after time instance t_2^Γ . It is obvious that t_5 is the next identifiable instance after time instance t_2^Γ . This time instance is designated as the time at which the input pattern I is withdrawn from the F_1 field of the AART1-NN. If the interval $[t_2^\Gamma, t_5]$ is long enough, then we are dealing with the fast learning case; otherwise we are dealing with the slow learning case.

It should be mentioned that additional AART1-NN parameter constraints were implied throughout the proof of Statement 2. Specifically, constraints CON16 and CON17 of Table III. These constraints impose a lower bound on the forcing terms affecting (A.1) and (A.6). If the forcing terms in these equations do not exceed the lower bound, then the activities of the F_1 field and reset nodes will never exceed their quenching thresholds.

Concluding, we can state that we have derived constraints CON1–CON17 of Table III under which we proved the validity of Statement 2. The validity of Statement 2 proves that the AART1-NN is capable of behaving in a manner identical to that of the ART1-NN.

V. PARAMETER CHOICES

Now that we have developed the AART1-NN parameter constraints listed in Table III, it is instructive to demonstrate how parameter values can be chosen for an example network. But first we mention some estimates of the quantities O_{\max} and O_{\min} that appear in CON1–CON17 of Table III. O_{\max} is an upper bound on the O_j 's for any pattern I that is presented at the F_1 field of the AART1-NN. A loose estimate of O_{\max} is $D_2 M$. A better estimate of O_{\max} is desirable; otherwise, CON11b of Table III will require unreasonably large values for the parameters B_2 and C_2 . In the fast learning case it can be shown that a better estimate of O_{\max} is $\frac{D_2 L M}{L-1+M}$. In the slow learning case, and under the assumption that $L = 1 + \sigma$ with $\sigma \ll 1$, it can be shown that a better estimate of O_{\max} is D_2 . O_{\min} is a lower bound on the O_j 's for any input pattern I that is presented at the F_1 field of the AART1-NN. Unless we have a better estimate for O_{\min} , based on some prior knowledge of the set of input patterns considered, it is always safe to take $O_{\min} = 0$ in CON1–CON17.

The sample network considered here contains four nodes in the F_1 field (nodes v_1 through v_4), a reset node (node v_r), and eight nodes in the F_2 field (nodes v_5 through v_8 in the first layer, and inhibitory nodes \hat{v}_5 through \hat{v}_8 in the second layer). Consequently for the sample network $M = 4$ and $N - M = 4$. We initially choose $L = 1.01$. This yields the estimate $O_{\max} = D_2$. Subsequently, we choose $A_1 = 1$, $D_1 = 1$, $\epsilon_1 = 0.001$, $\delta_1 = 0.01$, $\epsilon_r = 0.001$, $D_2 = 1$, $\epsilon_2 = 0.01$, $\delta_2 = 0.01$, and $\epsilon_z = 1$. These parameters can be thought of as being the “free parameters” in the network, despite the fact that they have to satisfy constraints CON1–CON17. We refer to them as “free parameters” due to the fact that they are picked first.

Now we choose the remaining AART1-NN parameter values so as to satisfy CON1–CON17. We first choose B_1 and C_1 values to satisfy CON2, CON3, CON7 and CON12; the reader can verify that $B_1 = 0.5$ and $C_1 = 100$ satisfy these constraints. We then choose $A_2 = 0.3$, having in mind CON2, CON13 and CON14. Furthermore, we choose B_2 and C_2 in a way that satisfies constraints CON2, CON3, CON9, CON10, and CON11. In our example, we chose $B_2 = 10000$ and $C_2 = 10000$; it is easy for the reader to verify that CON2, CON3, CON9, CON10, and CON11 are satisfied. Finally, we pick $\delta_r = 0.02$ and $A_r = 2$ so as to satisfy CON8, CON15, and CON17. Based on the aforementioned AART1-NN parameter values, we chose the initial bottom-up traces, the $z_{ij}(0)$'s, in the interval $(0, 0.251)$ and the initial top-down traces, the $z_{ji}(0)$'s, in the interval $(0.526, 1]$ (see CON5 and CON6). As a rule of thumb, in order to satisfy AART1-NN parameter constraints CON1–CON17, we choose the parameter values to make p_3 and e_6 as small as possible; p_8 , e_2 , and e_3 as large as possible; p_5 , p_6 , and p_7 as close to one as possible; p_4 as close to δ_1 as possible; and finally, p_2 as much larger than δ_1 as possible.

The AART1-NN parameter values chosen for this example are listed in Table IV. Some of the parameter values did not have any effect on the successful operation of the network, and as a result were chosen arbitrarily (e.g., $\hat{\delta}_2 = 0.0001$, $K = 1$). Furthermore the vigilance parameter ρ was selected to be equal to 1. Note that the AART1-NN should operate successfully for all the values of the vigilance parameter designated in CON4. Once more, the AART1-NN parameter values listed in Table IV satisfy all the constraints of Table III. Note though that the test for the validity of CON14 is computationally intensive for the fast learning case and almost impossible for the slow learning case. But it is worth observing that for the parameters chosen (i.e., $A_2 = 0.3$, and $O_{\max} = 1$) CON14 is satisfied if $O_{M+n+1} < 0.99979 O_{M+n}$ for $n = 2, \dots, N - M - 1$. Thus, in this case, the AART1-NN will satisfy CON14 for most O_j values of interest. Observe also that the ART1-NN, as defined in [1], operates successfully only when the O_j 's are distinct.

VI. COMPUTER SIMULATION

In this section we demonstrate the behavior of the AART1 model for both the fast and slow learning cases. As mentioned in Section V, the sample network considered here contains four nodes in the F_1 field (nodes v_1 through v_4), a reset node (node v_r), and eight nodes in the F_2 field (nodes v_5

TABLE IV
AART1-NN PARAMETER VALUES FOR THE EXAMPLE NETWORK

$A_1 = 1$	$B_1 = 0.5$	$C_1 = 100$	$D_1 = 1$	$\epsilon_1 = 0.001$
$\delta_1 = 0.01$	$A_r = 2$	$\epsilon_r = 0.001$	$\delta_r = 0.02$	$\rho = 1$
$A_2 = 0.3$	$B_2 = 10000$	$C_2 = 10000$	$D_2 = 1$	$\epsilon_2 = 0.01$
$\delta_2 = 0.01$	$\delta_2 = 0.0001$	$K = 1$	$L = 1.01$	$\epsilon_r = 1$

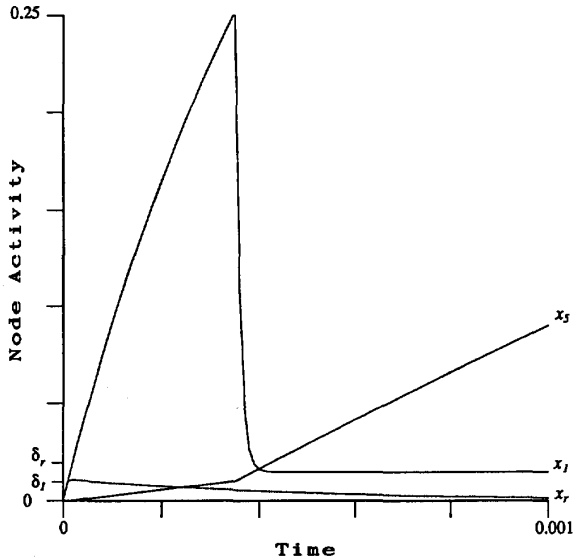


Fig. 3. Node activities during the presentation of pattern I^1 . The sudden drop in activity x_1 is a manifestation of the 2/3 rule in ART1.

through v_8 in the first layer, and inhibitory nodes \hat{v}_5 through \hat{v}_8 in the second layer). The node differential equations were numerically approximated using the fourth order Runge-Kutta method with a step size of 10^{-6} . Three patterns were presented to the network: $I^1 = 1000$, $I^2 = 0000$, and $I^3 = 1100$. Note that I^2 is the zero pattern used between presentation of other "interesting" patterns. That is, the presentation of pattern I^2 can be interpreted as the absence of an input pattern. The parameters chosen for the simulation of the sample network in both the fast and slow learning cases are shown in Table IV. The LTM traces for these simulations were selected so that $z_{ji}(0) = 1$, and $0 < z_{ij}(0) < \frac{L}{L-1+M}$ for all i, j . In addition, the bottom-up LTM traces were chosen so that when pattern I^1 is initially presented, v_5 receives the largest bottom-up input. Furthermore, when pattern I^3 is initially presented, v_5 receives the largest bottom-up input, and v_6 receives the next largest bottom-up input.

The behavior of the AART1-NN during the presentation of patterns I^1 , I^2 , and I^3 is described with reference to Figs. 3–7, which depict node activities versus time. Although time is a continuous parameter, it also has a meaning in terms of the number of steps elapsed during the approximation of the network differential equations. For the network simulations described in this section, time t corresponds to $10^6 \cdot t$ steps.

The fast learning case is examined first. Pattern $I^1 = 1000$ is presented to the network at time $t = 0$. The behavior of the network immediately following the presentation of I^1 is depicted in Fig. 3. Among the F_1 field nodes, only v_1 is of

interest because it is the only node receiving bottom-up input. After the input pattern is presented, the activity of v_1 increases from zero to a positive value above the threshold δ_1 . Once v_1 becomes supraliminally active, nodes in the first layer of the F_2 field begin to receive bottom-up input. Because v_5 receives the largest bottom-up input, it becomes supraliminally active before any other node in the first layer of the F_2 field. At this point, v_1 is receiving both bottom-up input, and strong top-down input from v_5 . This causes the activity of v_1 to decrease and subsequently reach a limiting value that is above the threshold δ_1 . Thus, node v_1 remains supraliminally active. Furthermore, the activity of v_5 continues to increase over the time interval depicted in Fig. 3. Recall that once v_5 becomes supraliminally active, it will inhibit the other nodes in the first layer of the F_2 field, forcing them to remain subliminally active as long as it remains supraliminally active. The activity of the reset node v_r in Fig. 3 should also be noted. Immediately after the presentation of I^1 , the activity x_r increases due to the mismatch between the output activity across the F_1 field, which equals zero, and the input pattern I^1 . Notice that the output activity across the F_1 field becomes equal to I^1 before the activity of the reset node exceeds its threshold δ_r . From this point on, the activity of the reset node decays towards its limiting value of zero. That is, even after the activation of v_5 , the activity x_r continues to decrease, due to the fact that there is no mismatch between bottom-up and top-down inputs across the F_1 field. Pattern I^1 is presented until time $t = 3.0$. This allows the bottom-up and top-down LTM traces to approximately reach their limiting values.

At time $t = 3.0$ pattern $I^2 = 0000$ is presented to the network. The behavior of the network after the appearance of pattern I^2 is shown in Fig. 4. Initially v_1 is at an activity level above the threshold δ_1 , but its activity drops to a level below δ_1 almost instantaneously. This results from v_1 receiving only top-down input (prior to time $t = 3.0$ it was receiving bottom-up and strong top-down input). After the deactivation of v_1 , the activity levels of nodes v_1 and v_2 stay at a constant level until v_5 is deactivated. The activity x_1 is larger than the activity x_2 because node v_1 receives stronger top-down input than v_2 . In the meantime, the activity of v_5 drops from a positive value to zero. Once v_5 becomes subliminally active, the activities of v_1 and v_2 decrease to zero because they are no longer receiving top-down input. The activity of v_6 starts increasing from a negative value towards zero immediately after v_5 becomes subliminally active. The behavior of v_6 is not fully depicted in Fig. 4 because its activity is significantly negative (≈ -1.0) when v_5 becomes subliminally active. Pattern I^2 is held at the network input until time $t = 3.2$.

At time $t = 3.2$ pattern $I^3 = 1100$ is presented. The behavior of the network after the presentation of I^3 is depicted in Figs. 5 and 6. In Fig. 5, after the presentation of I^3 , v_5 becomes supraliminally active before any other node in the first layer of the F_2 field because it receives the largest bottom-up input from the F_1 field. Once v_5 becomes supraliminally active, the activities of nodes v_1 and v_2 begin to decrease. The activity of v_1 remains above the threshold δ_1 , while the activity of v_2 decreases to a level below δ_1 . This is a consequence of v_1 receiving strong top-down input, while v_2

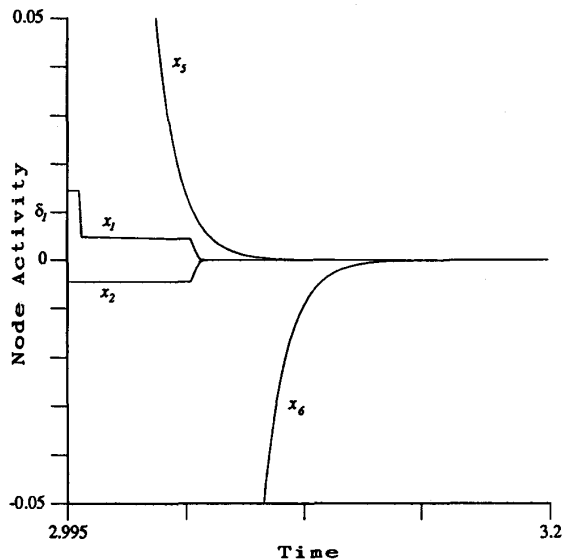


Fig. 4. Node activities during the presentation of pattern I^2 .

receives weak top-down input—both nodes receive bottom-up input. When v_2 becomes subliminally active, the activity of the reset node starts increasing due to the mismatch between the bottom-up and top-down inputs that is now occurring at the F_1 field. When v_r becomes supraliminally active (i.e., its activity exceeds δ_r) it generates a reset wave that deactivates v_5 almost instantaneously. After v_5 becomes subliminally active, v_1 and v_2 receive only bottom-up input, and their activities increase towards the limiting value of 0.5 (see Fig. 6). Now that v_5 is deactivated, v_6 will become supraliminally active next since it is the node in the first layer of the F_2 field that receives the next largest bottom-up input from the F_1 field. That is, v_6 will be activated before any other eligible node (v_7 or v_8) in the first layer of the F_2 field. The activation of v_6 is shown in Fig. 6. When v_6 becomes supraliminally active, the activities of nodes v_1 and v_2 begin to decrease from the value 0.5; but they remain above the quenching threshold δ_1 . This is a consequence of both v_1 and v_2 receiving bottom-up input and strong top-down input. Notice also that the activity of the reset node starts decreasing some time after the deactivation of v_5 (see Fig. 5), and that it continues to do so after the activation of v_6 (see Fig. 6) because there is no mismatch between bottom-up and top-down inputs at the F_1 field. Hence, when pattern I^3 is held at the network inputs long enough, the bottom-up and top-down LTM traces reach their limiting values.

We now consider the slow learning case. First, pattern I^1 is presented at time $t = 0$, and the network exhibits the behavior depicted in Fig. 3. However, in this case, soon after v_5 wins the competition in the first layer of the F_2 field, pattern I^1 is removed from the network inputs. Thus, the bottom-up and top-down LTM traces are not allowed to converge to their limiting values. Pattern I^1 is presented until time $t = 0.1$, and then pattern $I^2 = 0000$ is presented. By time $t = 0.3$, all node activities have converged to their resting values of zero. The behavior of the network during the presentation of

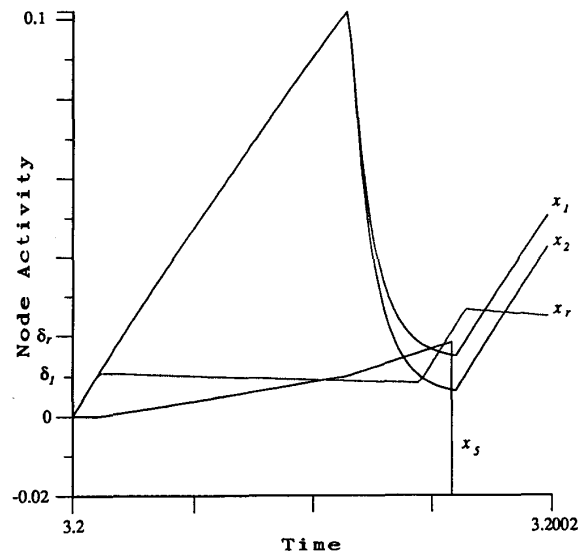


Fig. 5. Node activities leading to a reset during the presentation of pattern I^3 . The sudden drop in activities x_1 and x_2 is again a manifestation of the 2/3 rule in ART1. Note that the activity of node v_1 remains supraliminally active, while node v_2 becomes subliminally active. Because of the choice of the ρ parameter, this causes the activity of the reset node v_r to become supraliminally active, and leads to a reset of node v_5 .

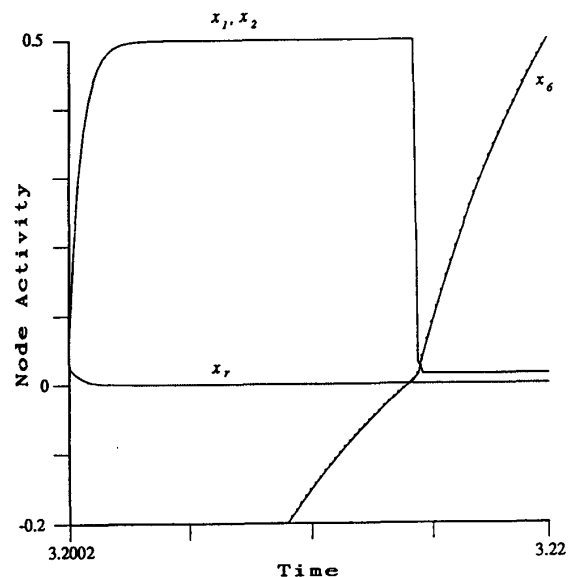


Fig. 6. Node activities after the reset during the presentation of pattern I^3 .

pattern I^2 is similar to that shown in Fig. 4, with the time instances 3.0 and 3.2 now corresponding to time instances 0.1 and 0.3. The major difference between the fast and slow learning cases demonstrated in these simulations occurs when pattern I^3 is presented to the network at time $t = 0.3$. The behavior of the network after the presentation of pattern I^3 is depicted in Fig. 7. It is instructive to compare Figs. 5 and 6, the network behavior in the fast learning case after pattern I^3 is presented, with Fig. 7. As in the fast learning case, v_5

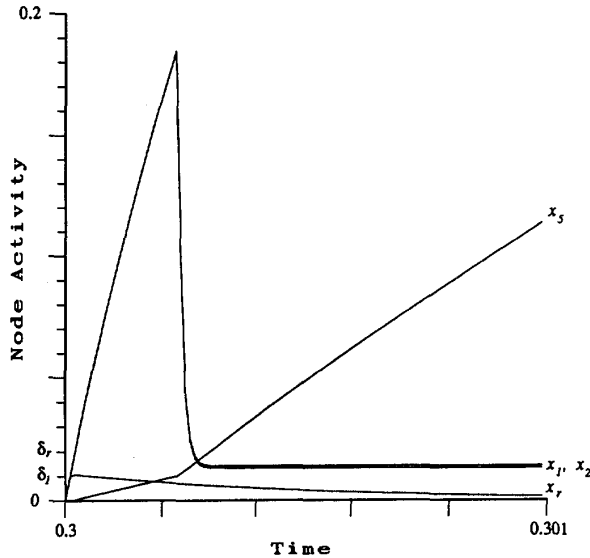


Fig. 7. Node activities after the presentation of pattern I^3 , when pattern I^1 has not been coded by v_5 on a previous pattern presentation.

receives the largest bottom-up input. Hence, v_5 is activated prior to any other node in the first layer of the F_2 field. This activation forces the activities of nodes v_1 and v_2 to decrease to limiting values that remain above the threshold value δ_1 . In the slow learning case, the fact that x_2 remains above δ_1 while pattern I^3 is presented is a consequence of not allowing the top-down traces leading to v_5 to approach their equilibrium values during the presentation of pattern I^1 . As a result, when v_5 becomes supraliminally active, nodes v_2 and v_1 receive bottom-up input and strong top-down input. Thus, since both v_1 and v_2 stay supraliminally active, v_5 is not reset. That is, the reset node remains subliminally active throughout the time that pattern I^3 is presented. Therefore, if pattern I^3 is held at the network inputs long enough, the LTM traces of node v_5 will approach their limiting values.

VII. CONCLUSIONS

The contribution of our work is twofold. First, we extended the ART1-NN model by both introducing new, and modifying already existing ART1 differential equations. This dynamical system model was denoted the AART1-NN. The distinguishing feature of the AART1-NN is that it incorporates all of the ART1 mechanisms into a set of coupled nonlinear differential equations. Second, we rigorously analyzed the AART1-NN equations and showed that they exhibit an ART1-NN behavior, as it is documented in [1, sections 3–6]. Although it is implied in [1] that the ART1 model can be implemented in this fashion, a thorough justification is not provided. This work demonstrates how the ART1 model can be cast into the form of a nonlinear dynamical system, and supplies a method for proving that this dynamical system will exhibit the behavior of the ART1 model. Furthermore, the capability of implementing the ART1 model in this fashion is of practical importance because it allows the tools used in the analysis of nonlinear

dynamical systems to be applied (see the discussion in Section I). Finally, the method applied to analyze the STM and LTM dynamics of the AART1-NN can be extended to other neural network models where the network dynamics are described via a set of nonlinear differential equations.

APPENDIX A

In this appendix we present a number of AART1-NN equations that are instrumental to the proof of Statement 2. The activity of a node v_i that receives bottom-up input, and no top-down input, satisfies the following equation for $t \in (t_a, t_b]$:

$$x_i(t) = x_i(t_a) \exp[-(1 + A_1)\epsilon_1^{-1}(t - t_a)] + \frac{1}{1 + A_1} [1 - \exp[-(1 + A_1)\epsilon_1^{-1}(t - t_a)]]. \quad (\text{A.1})$$

The above equation is obtained by solving equation (2) in the main text with $J_i^+ = 1$ and $J_i^- = 0$.

The activity of a node v_i that receives bottom-up input, as well as top-down input from a node v_j satisfies the following equation for $t \in (t_a, t_b]$:

$$x_i(t) = x_i(t_a) \exp[-(1 + A_1 + D_1 A_1 z_{ji} + C_1)\epsilon_1^{-1}(t - t_a)] + \frac{1 + D_1 z_{ji} - B_1}{1 + A_1 + D_1 A_1 z_{ji} + C_1} \times [1 - \exp[-(1 + A_1 + D_1 A_1 z_{ji} + C_1)\epsilon_1^{-1}(t - t_a)]]. \quad (\text{A.2})$$

The above equation is derived by solving (2) with $J_i^+ = 1 + D_1 z_{ji}$ and $J_i^- = 1$. In the above equation, the case where $\frac{1 + D_1 z_{ji} - B_1}{1 + A_1 + D_1 A_1 z_{ji} + C_1} > \delta_1$ can be distinguished from the case where $\frac{1 + D_1 z_{ji} - B_1}{1 + A_1 + D_1 A_1 z_{ji} + C_1} \leq \delta_1$. In the former case, we say that node v_i receives bottom-up input and strong top-down input from node v_j . In the latter case, we say that node v_i receives bottom-up input and weak top-down input from node v_j .

The activity of a node v_j that receives a bottom-up input T_j from the F_1 field over a time interval in which no node in the first layer of the F_2 field is supraliminally active, satisfies the following equation for $t \in (t_a, t_b]$:

$$x_j(t) = x_j(t_a) \exp[-(1 + A_2 T_j)\epsilon_2^{-1}(t - t_a)] + \frac{T_j}{1 + A_2 T_j} [1 - \exp[-(1 + A_2 T_j)\epsilon_2^{-1}(t - t_a)]]. \quad (\text{A.3})$$

The above equation is obtained by solving (6) with $J_j^+ = T_j$ and $J_j^- = 0$.

The activity of a node v_j that receives a bottom-up input T_j from the F_1 field over a time interval in which another node in the first layer of the F_2 field is supraliminally active, satisfies the following equation for $t \in (t_a, t_b]$:

$$x_j(t) = x_j(t_a) \exp[-(1 + A_2 T_j + C_2)\epsilon_2^{-1}(t - t_a)] + \frac{T_j - B_2}{1 + A_2 T_j + C_2} \times [1 - \exp[-(1 + A_2 T_j + C_2)\epsilon_2^{-1}(t - t_a)]]. \quad (\text{A.4})$$

The above equation is derived by solving (6) with $J_j^+ = T_j$ and $J_j^- = 1$.

The activity of the only supraliminally active node v_j that receives a bottom-up input T_j from the F_1 field satisfies, after the initiation of a reset wave by the reset node v_r , the following equation:

$$\frac{d}{dt}x_j = -(1 + A_2 + A_2T_j + C_2)\epsilon_2^{-1}x_j + (1 + T_j - B_2)\epsilon_2^{-1}. \quad (\text{A.5})$$

The above equation is derived from (6) by substituting J_j^+ with $1 + T_j$ and J_j^- with 1.

The activity of the reset node v_r , if there is a mismatch between the input pattern I and the output activity across the F_1 field, satisfies the following equation for $t \in (t_a, t_b)$:

$$x_r(t) = x_r(t_a)\exp[-A_r\epsilon_r^{-1}(t - t_a)] + \frac{1}{A_r}[1 - \exp[-A_r\epsilon_r^{-1}(t - t_a)]]. \quad (\text{A.6})$$

The above equation is obtained by solving (18) with

$$U \left[P \sum_{i=1}^M I_i - Q \sum_{i=1}^M f_1(x_i) \right] = 1.$$

If there is no mismatch between I and the output activity across the F_1 field over this interval, then the activity of the reset node satisfies

$$x_r(t) = x_r(t_a)\exp[-A_r\epsilon_r^{-1}(t - t_a)]. \quad (\text{A.7})$$

The above equation is obtained by solving (18) with

$$U \left[P \sum_{i=1}^M I_i - Q \sum_{i=1}^M f_1(x_i) \right] = 0.$$

APPENDIX B

In this appendix we show that by choosing the AART1-NN parameter values according to CON8 we can guarantee that the reset node is subliminally active at time instance t_1^0 . The activity of a node v_i that receives bottom-up inputs in the interval $(t_0, t_1^0]$ satisfies (A.1) with $t_a = t_0$ and $x_i(t_a) = x_i(t_0) = 0$. At time instance $t = t_1^0$, $x_i(t) = x_i(t_1^0) = \delta_1$. Thus,

$$t_1^0 - t_0 = \frac{-\ln\{1 - \delta_1(1 + A_1)\}\epsilon_1}{1 + A_1}.$$

Since the activity of the reset node v_r in the time interval $(t_0, t_1^0]$ satisfies (A.6) with $t_a = t_0$ and $x_r(t_a) = x_r(t_0) = 0$, the activity of the reset node at time instance $t = t_1^0$ is given by

$$x_r(t_1^0) = \frac{1 - [1 - \delta_1(1 + A_1)]^{\frac{A_r\epsilon_1}{(1+A_1)\epsilon_r}}}{A_r}.$$

Therefore, by choosing the AART1-NN parameter values as in CON8 we can guarantee that the reset node is subliminally active at time instance t_1^0 .

APPENDIX C

In this appendix we provide an example where in the second competition cycle, corresponding to the presentation of an input pattern I at the F_1 field of the AART1-NN, $T_{M+2} = 0$ and $T_{M+3} = O_{M+3}$. The network under consideration consists of eight nodes in the F_1 field (i.e., nodes v_1 through v_8), and four nodes in the first and second layer of the F_2 field (i.e., nodes v_9 through v_{12} in the first layer, and nodes \hat{v}_9 through \hat{v}_{12} in the second layer). Consequently, in this sample network $M = 8$ and $N - M = 4$. The vigilance parameter ρ is chosen to be 1. Let us assume that the input patterns are presented long enough at the F_1 field of the AART1-NN so that fast LTM learning occurs. Let us also assume that prior to the presentation of the input pattern I , the network has already learned the input patterns $I_1 = 00001111$, $I_2 = 01110000$, and $I_3 = 00001100$. In particular, the LTM bottom-up and top-down traces of node v_9 are equal to 0000aaaa and 00001111, respectively, where $a = L\{L - 1 + 4\}^{-1}$. Furthermore, the LTM bottom-up and top-down traces of node v_{10} are equal to 0bbb0000 and 01110000, respectively, where $b = L\{L - 1 + 3\}^{-1}$. Finally, the LTM bottom-up and top-down traces of node v_{11} are equal to 0000cc00 and 00001100, where $c = L\{L - 1 + 2\}^{-1}$. In short, node v_9 has learned the input pattern I_1 , node v_{10} has learned the input pattern I_2 , and node v_{11} has learned the input pattern I_3 .

We now present pattern $I = 01111111$ at the F_1 field of the AART1-NN. We assume that the network parameters are chosen so that $O_9 > O_{10} > O_{11} > O_{12}$. As a result, node v_9 in the first layer of the F_2 field will be activated first, and it will be reset since $\rho = 1$. Time instance t_4^1 has been designated as the time at which node v_9 is deactivated; at this time the second competition cycle starts. In the time interval (t_4^1, t_1^1) , it is easy to see that the output activity across the F_1 field is equal to 00001111. Consequently, in the time interval (t_4^1, t_1^1) the bottom-up input T_{10} (i.e., T_{M+2}) is equal to zero, while the bottom-up input T_{11} (i.e., T_{M+3}) is equal to O_{M+3} . This demonstrates our point.

APPENDIX D

Appendix D.1

In this appendix we prove that by choosing the AART1-NN parameter values according to CON11 we can guarantee that $x_j(t_4^1)$ in (27) is approximately equal to its minimum value of $-B_2C_2^{-1}$. Let us examine the interval (t_2^1, t_4^1) . Within this interval there is at least one node in the F_1 field that receives bottom-up and weak top-down signals. We assume, without loss of generality, that node v_1 is the first node in the F_1 field that becomes subliminally active after time instance t_2^1 . Let us denote by $t_2^1 + \Delta t_1$ the time at which node v_1 becomes subliminally active. In the time interval $(t_2^1, t_2^1 + \Delta t_1)$, the activity of the node v_j ; ($j \neq M + 1$) satisfies (A.4) with $t_a = t_2^1$ and $T_j = O_j$. If we show that at time $t_2^1 + \Delta t_1$ the activity of a node v_j ; ($j \neq M + 1$) is, by appropriately choosing the AART1-NN parameters, upper-bounded by $\epsilon\theta + (-B_2C_2^{-1})(1 - \theta)$ for ϵ and θ small positive constants, and ϵ small compared to $B_2C_2^{-1}$, then we have

shown that $x_j(t_4^1)$ is approximately equal to its minimum value of $-B_2C_2^{-1}$. This is true because the activity of a node v_j ($j \neq M+1$) continues to decrease after time $t_2^1 + \Delta t_1$ and until time t_4^1 , and because the activities of all the nodes in the first layer of the F_2 field are lower bounded by $-B_2C_2^{-1}$.

Let us first determine Δt_1 . In the time interval $(t_2^1, t_2^1 + \Delta t_1)$ the activity of the node v_1 satisfies (A.2) with $t_a = t_2^1$, and $z_{ji} = z_{M+1,1}$. The quantity Δt_1 is found by setting $x_1(t_2^1 + \Delta t_1)$ equal to δ_1 in (A.2). This yields

$$\Delta t_1 = \frac{\ln(\Psi_2)\epsilon_1}{1 + A_1 + D_1A_1z_{M+1,1} + C_1},$$

with

$$\Psi_2 = \frac{-(1 + D_1z_{M+1,1} - B_1) + x_1(t_2^1)(1 + A_1 + D_1A_1z_{M+1,1} + C_1)}{-(1 + D_1z_{M+1,1} - B_1) + \delta_1(1 + A_1 + D_1A_1z_{M+1,1} + C_1)}.$$

Furthermore, the activity of node v_j ($j \neq M+1$) at time $t_2^1 + \Delta t_1$ will be given by (A.4) if we substitute $x_j(t_a)$ with $x_j(t_2^1)$, $t - t_a$ with Δt_1 from above, and T_j with O_j . This yields

$$x_j(t_2^1 + \Delta t_1) = x_j(t_2^1)\Psi_3^{\frac{(1+A_2O_j+C_2)\epsilon_1}{(1+A_1+D_1A_1z_{M+1,1}+C_1)\epsilon_2}} + \frac{O_j - B_2}{1 + A_2O_j + C_2} \times \left\{ 1 - \Psi_3^{\frac{(1+A_2O_j+C_2)\epsilon_1}{(1+A_1+D_1A_1z_{M+1,1}+C_1)\epsilon_2}} \right\}, \quad (\text{D.1})$$

where $\Psi_3 = \Psi_2^{-1}$. Since Ψ_3 is greater than zero and $x_j(t_2^1) < \delta_2$; ($j \neq M+1$), an upper bound for the right hand side of (D.1) is found if $x_j(t_2^1)$ is substituted with its upper bound δ_2 . Furthermore, let us choose the AART1-NN parameters in a way that allows us to approximate the term $(O_j - B_2)(1 + A_2O_j + C_2)^{-1}$ with the term $-B_2C_2^{-1}$. It is not difficult to see that we can accomplish this goal by choosing the AART1-NN parameters according to CON11a and CON11b in Table III. Consequently, we can now state that

$$x_j(t_2^1 + \Delta t_1) < \delta_2\Psi_3^{\frac{(1+A_2O_j+C_2)\epsilon_1}{(1+A_1+D_1A_1z_{M+1,1}+C_1)\epsilon_2}} + (-B_2C_2^{-1}) \times \left\{ 1 - \Psi_3^{\frac{(1+A_2O_j+C_2)\epsilon_1}{(1+A_1+D_1A_1z_{M+1,1}+C_1)\epsilon_2}} \right\}. \quad (\text{D.2})$$

In Appendix D.2 we show that Ψ_3 decreases as $z_{M+1,1}$ increases. Furthermore, in Appendix D.3 we demonstrate that $x_1(t_2^1)$ is lower bounded by p_2 , where p_2 is given in Table V. These two facts allow us to state that Ψ_3 is upper bounded by p_3 which is also defined in Table V. Finally, it is easy to see that the exponent of Ψ_3 in (D.2) is lower bounded by the value for e_3 given in Table V. Combining all of the aforementioned facts we have from (D.2) that

$$x_j(t_2^1 + \Delta t_1) < \delta_2 p_3^{e_3} + (-B_2C_2^{-1})(1 - p_3^{e_3}). \quad (\text{D.3})$$

The upper bound on $x_j(t_2^1 + \Delta t_1)$ in (D.3) is in the desired form, provided that CON11c and CON11d are satisfied. In

TABLE V
DEFINITION OF PARAMETERS APPEARING IN CON1 -CON17

O_{\max}	an upper bound of $O_{M+1}, O_{M+2}, \dots, O_{N-M}$
O_{\min}	a lower bound of $O_{M+1}, O_{M+2}, \dots, O_{N-M}$
n	index of the competition cycle; $n \in \{2, 3, \dots, N - M - 1\}$
p_1	a positive number \gg than 1
p_2	$\delta_1(1 - \delta_2A_2 - \delta_2O_{\max}^{-1})^n + [1 - (1 - \delta_2A_2 - \delta_2O_{\max}^{-1})^n] \delta_1(1 + A_1)^{-1}$
p_3	$\frac{-(1 - B_2)\epsilon_1(1 + A_1 + C_1)}{-(1 - B_2)\epsilon_1(1 + A_1 + C_1)}$
p_4	$(1 - B_2)(1 + A_1 + C_1)^{-1}$
p_5	$p_2^n + (1 - p_2^n)(1 + A_2O_{\max})^{-1}$
p_6	$[1 - \delta_1(1 + A_1)] [1 - p_2(1 + A_1)]^{-1}$
p_7	$p_2[1 + (1 - p_2)A_2O_{\max}]^{-1}$
p_8	$\frac{1 + 2z_{M+1,1}}{A_2}$
e_2	δ_1
e_3	$\frac{[(1 + A_1)\epsilon_2] [(1 + A_2O_{\max})\epsilon_1]^{-1}}{[(1 + A_2O_{\min} + C_2)\epsilon_1] [(1 + A_1 + D_1A_1 + C_1)\epsilon_2]^{-1}}$
e_8	e_2^{-1}

review, we have demonstrated in this appendix that under CON11 we can state that $x_j(t_4^1) \approx -B_2C_2^{-1} = -O_{\max}$; ($j \neq M+1$).

Appendix D.2:

In this appendix we show that Ψ_3 , defined in Appendix D.1, decreases as $z_{M+1,1}$ increases. The quantity Ψ_3 was defined in Appendix D.1 as

$$\Psi_3 = \frac{-(1 + D_1z_{M+1,1} - B_1) + \delta_1(1 + A_1 + D_1A_1z_{M+1,1} + C_1)}{-(1 + D_1z_{M+1,1} - B_1) + x_1(t_2^1)(1 + A_1 + D_1A_1z_{M+1,1} + C_1)}.$$

Let us evaluate the derivative of Ψ_3 with respect to $z_{M+1,1}$. The derivative of Ψ_3 with respect to $z_{M+1,1}$ is a ratio. The denominator of this ratio is a positive number. If the numerator of this ratio is negative then we have proven that Ψ_3 decreases as $z_{M+1,1}$ increases. Let us examine the numerator of $\frac{d\Psi_3}{dz_{M+1,1}}$:

$$\begin{aligned} & (-D_1 + \delta_1D_1A_1)[-(1 + D_1z_{M+1,1} - B_1) \\ & + x_1(t_2^1)(1 + A_1 + D_1A_1z_{M+1,1} + C_1)] \\ & + (D_1 - x_1(t_2^1)D_1A_1)[-(1 + D_1z_{M+1,1} - B_1) \\ & + \delta_1(1 + A_1 + D_1A_1z_{M+1,1} + C_1)] \\ & = [x_1(t_2^1) - \delta_1]\{-D_1(1 + A_1 + D_1A_1z_{M+1,1} + C_1) \\ & + D_1A_1(1 + D_1z_{M+1,1} - B_1)\} \\ & < [x_1(t_2^1) - \delta_1]\{-D_1(1 + A_1 + D_1A_1z_{M+1,1} + C_1) \\ & + \delta_1D_1A_1(1 + A_1 + D_1A_1z_{M+1,1} + C_1)\} \\ & = D_1[x_1(t_2^1) - \delta_1](\delta_1A_1 - 1)(1 + A_1 + D_1A_1z_{M+1,1} + C_1). \end{aligned}$$

In the last expression derived above, $D_1 > 0$, $x_1(t_2^1) - \delta_1 > 0$ (because node v_1 is supraliminally active at time t_2^1), $\delta_1A_1 - 1 < 0$ (A_1^{-1} is the maximum activation value of a node in the F_1 field, and δ_1 is the threshold of the node), and $1 + A_1 + D_1A_1z_{M+1,1} > 0$. Consequently, the numerator of the derivative $\frac{d\Psi_3}{dz_{M+1,1}}$ is negative, which proves that Ψ_3 decreases as $z_{M+1,1}$ increases. The inequality utilized in the above derivations is justified because node v_1 is by assumption a node that receives bottom-up and weak top-down inputs, and as a result $1 + D_1z_{M+1,1} - B_1 < (1 + A_1 + D_1A_1z_{M+1,1} + C_1)\delta_1$.

Appendix D.3:

In this appendix we prove that $x_1(t_2^1) \geq p_2$, where p_2 is defined in Table V. Consider the interval (t_1^0, t_2^1) . In this

interval, the activity of every node v_i that receives bottom-up input, and hence the activity of node v_1 , satisfies (A.1) with $t_a = t_1^0$. Furthermore, in this interval, the activity of every node v_j satisfies (A.3) with $t_a = t_1^0$ and $T_j = O_j$. Since node v_{M+1} wins this competition cycle, we can write

$$t_2^1 - t_1^0 = \frac{\ln(\Psi_4)\epsilon_2}{1 + A_2O_{M+1}},$$

with

$$\Psi_4 = \frac{O_{M+1} - x_{M+1}(t_1^0)(1 + A_2O_{M+1})}{O_{M+1} - \delta_2(1 + A_2O_{M+1})}.$$

Due to the above equations, the activity of node v_1 at time instance t_2^1 is given by (A.1) if we substitute t_a with t_1^0 , and $t - t_a$ with $t_2^1 - t_1^0$ from above. This yields

$$x_1(t_2^1) = x_1(t_1^0)\Psi_5^{\frac{(1+A_1)\epsilon_2}{(1+A_2O_{M+1})\epsilon_1}} + \frac{1}{1 + A_1} \times \left\{ 1 - \Psi_5^{\frac{(1+A_1)\epsilon_2}{(1+A_2O_{M+1})\epsilon_1}} \right\}, \quad (\text{D.4})$$

where $\Psi_5 = \Psi_4^{-1}$. We are now ready to derive a lower bound for $x_1(t_2^1)$ of equation (D.4). Because $x_1(t_1^0) > \delta_1$ and $\Psi_5 > 0$, a lower bound on the right hand side of (D.4) can be found if we substitute $x_1(t_1^0)$ with δ_1 . The resulting lower bound can be lower bounded once more if we substitute Ψ_5 with one of its upper bounds, and the exponent of Ψ_5 with one of its lower bounds. This is due to the fact that $\frac{1}{1+A_1} > \delta_1$ (see CON16 in Table III), and $\Psi_5 < 1$. Note that $\Psi_5 < 1 - \delta_2A_2 - \delta_2O_{\max}^{-1}$, since $x_{M+1}(t_1^0) = 0$. Also, note that $(1 + A_1)\epsilon_2[(1 + A_2O_{M+1})\epsilon_1]^{-1} > (1 + A_1)\epsilon_2[(1 + A_2O_{\max})\epsilon_1]^{-1}$. The above discussion proves that p_2 of Table V is indeed a lower bound of $x_1(t_2^1)$.

APPENDIX E

In this appendix we prove the validity of ART1 design constraint #3 in the second competition cycle. In other words, we prove that node v_{M+2} is the first node to be activated after time instance t_1^1 . Consider the activity of node v_{M+2} and the activity of a node v_j ($j \neq M+1, M+2$) after time instance t_1^1 . The activity of both nodes, after time instance t_1^1 , is described by equation (A.3) with $t_a = t_1^1$ and $T_j = O_j$. If $x_{M+2}(t_1^1) \geq x_j(t_1^1)$, then node v_{M+2} will become supraliminally active before node v_j (note that $O_{M+2} > O_j$ for $j \neq M+1, M+2$). Let us concentrate therefore on the more interesting case where $x_{M+2}(t_1^1) < x_j(t_1^1)$, and in particular on the extreme case where $x_j(t_1^1) - x_{M+2}(t_1^1)$ is substituted by one of its upper bounds. This extreme case is derived below.

Assume that node v_{M+2} receives a bottom-up input $T_{M+2} = 0$ in the time interval (t_4^1, t_1^1) . Hence, the activity of node v_{M+2} in this interval satisfies (A.3) with $x_j(t_a) = x_{M+2}(t_4^1) \approx -O_{\max}$, $T_j = T_{M+2} = 0$, and $t - t_a = t_1^1 - t_4^1$, where $t_1^1 - t_4^1$ is given by (26). As a result, $x_{M+2}(t_1^1) = -O_{\max}\Psi_1^{\frac{(1+A_2O_j)\epsilon_1}{(1+A_1)\epsilon_2}}$, where Ψ_1 was defined in (28). We also assume that node v_j ($j \neq M+1, M+2$) receives a bottom-up input $T_j = O_j$ in the intervals (t_4^1, t_1^1) . Hence, the activity of v_j satisfies (A.3)

with $x_j(t_a) \approx -O_{\max}$, $T_j = O_j$, and $t - t_a = t_1^1 - t_4^1$, where $t_1^1 - t_4^1$ is given by (26). Consequently,

$$x_j(t_1^1) = -O_{\max}\Psi_1^{\frac{(1+A_2O_j)\epsilon_1}{(1+A_1)\epsilon_2}} + \frac{O_j}{1 + A_2O_j} \times \left\{ 1 - \Psi_1^{\frac{(1+A_2O_j)\epsilon_1}{(1+A_1)\epsilon_2}} \right\}. \quad (\text{E.1})$$

An upper bound on $x_j(t_1^1)$ can be found if the O_j 's in (E.1) are substituted with O_{\max} , and Ψ_1 is substituted with its lower bound of p_6 given in Table V. Note that p_4 in Table V is a lower bound on $x_1(t_4^1)$. Also, $-O_{\max}$ is a lower bound on $x_{M+2}(t_1^1)$. As a result, we can write that $x_j(t_1^1) < -p_5O_{\max}$, and $x_{M+2}(t_1^1) > -O_{\max}$, where p_5 is defined in Table V. Based on these inequalities, an upper bound on $x_j(t_1^1) - x_{M+2}(t_1^1)$ is given by the term $(1 - p_5)O_{\max}$, and this upper bound corresponds to the extreme case that we plan to consider. For this extreme case we will now determine conditions on the values of the bottom-up inputs O_j ($j \neq M+1$) so that node v_{M+2} will be activated before any other node v_j ($j \neq M+1, M+2$). Suppose first that node v_{M+2} becomes supraliminally active before any other node v_j ($j \neq M+2$) in the first layer of the F_2 field. This event will happen at time $t_1^1 + \Delta t_{M+2}$, where Δt_{M+2} is given by the following equation:

$$\Delta t_{M+2} = \ln \left[\frac{O_{M+2} - x_{M+2}(t_1^1)(1 + A_2O_{M+2})}{O_{M+2} - \delta_2(1 + A_2O_{M+2})} \right] \times \frac{\epsilon_2}{1 + A_2O_{M+2}}. \quad (\text{E.2})$$

Suppose now that node v_j ($j \neq M+1, M+2$) becomes supraliminally active before any other node in the first layer of the F_2 field. This event will happen at time $t_1^1 + \Delta t_j$, where Δt_j is given by the following equation:

$$\Delta t_j = \ln \left[\frac{O_j - x_j(t_1^1)(1 + A_2O_j)}{O_j - \delta_2(1 + A_2O_j)} \right] \frac{\epsilon_2}{1 + A_2O_j}. \quad (\text{E.3})$$

The equations for Δt_{M+2} and Δt_j were derived using equation (A.3). In order to prove the validity of ART1 design constraint #3 during the second competition cycle, we have to show that under certain AART1-NN parameter constraints, $\Delta t_{M+2} < \Delta t_j$. After substituting $x_{M+2}(t_1^1)$ with $-O_{\max}$, and $x_j(t_1^1)$ with $-p_5O_{\max}$ in (E.2) and (E.3), respectively, we arrive at

$$\Delta t_{M+2} = \ln \left[\frac{y_{M+2} + O_{\max}}{y_{M+2} - \delta_2} \right] \frac{\epsilon_2}{1 + A_2O_{M+2}}$$

and

$$\Delta t_j = \ln \left[\frac{y_j + p_5O_{\max}}{y_j - \delta_2} \right] \frac{\epsilon_2}{1 + A_2O_j}$$

where $y_{M+2} = \frac{O_{M+2}}{1 + A_2O_{M+2}}$ and $y_j = \frac{O_j}{1 + A_2O_j}$. Based on the above equations, it is easy to see that a sufficient condition for Δt_{M+2} to be smaller than Δt_j , for $j \neq M+1, M+2$, is the following:

$$\frac{y_{M+2} + O_{\max}}{y_{M+2} - \delta_2} < \frac{y_j + p_5O_{\max}}{y_j - \delta_2}.$$

Multiplying both sides of the above inequality with $(y_{M+2} - \delta_2)(y_j - \delta_2)$, yields an equivalent inequality:

$$\begin{aligned} & -\delta_2 y_{M+2} + y_j O_{\max} - \delta_2 O_{\max} \\ & < -\delta_2 y_j + p_5 y_{M+2} O_{\max} - p_5 \delta_2 O_{\max}. \end{aligned}$$

To satisfy this inequality it suffices to guarantee that $y_j < p_5 y_{M+2}$. This is because $-\delta_2 y_{M+2} - \delta_2 O_{\max} < -\delta_2 y_j - p_5 \delta_2 O_{\max}$. Substituting y_j and y_{M+2} with their equals of $O_j(1 + A_2 O_j)^{-1}$, and of $O_{M+2}(1 + A_2 O_{M+2})^{-1}$, we arrive at the condition

$$p_5 O_j^{-1} - O_{M+2}^{-1} > (1 - p_5) A_2.$$

A sufficient condition for the satisfaction of this inequality is constraint CON14 of Table III. Consequently, we have proven that ART1 design constraint #3 is valid in the second competition cycle, provided that CON14 is satisfied.

APPENDIX F

In this appendix we will prove that under certain AART1-NN design constraints, the reset node becomes subliminally active by time instance t_2^2 , and as a result ART1 design constraint #4 is satisfied in the second competition cycle. Note that at time instance t_2^2 , there is no mismatch between bottom-up and top-down inputs at the F_1 field.

Assume we are at time instance t_1^1 , and that the reset node is deactivated at some point prior to time instance t_2^2 . We will develop appropriate AART1-NN constraints that prove the correctness of the latter assumption. After time instance t_1^1 the activity of the reset node satisfies (A.7) with $t_a = t_1^1$. Based on (A.7) we can show that the reset node is deactivated at time $t_1^1 + \Delta t_{r1}$, where $\Delta t_{r1} = \ln[x_r(t_1^1) \delta_r^{-1}] A_r^{-1} \epsilon_r$. If we can demonstrate that under certain AART1-NN parameter constraints, the activity of every node v_j ($j \neq M+1$) at time $t_1^1 + \Delta t_{r1}$ is below δ_2 , then we have proven ART1 design constraint #4. The activity of a node v_j ($j \neq M+1$) after t_1^1 satisfies (A.3) with $t_a = t_1^1$ and $T_j = O_j$. Hence, at time $t_1^1 + \Delta t_{r1}$ we can state that

$$\begin{aligned} x_j(t_1^1 + \Delta t_{r1}) &= x_j(t_1^1) \Psi_6 \frac{(1 + A_2 O_j) \epsilon_r}{A_r \epsilon_2} \\ &+ \frac{O_j}{1 + A_2 O_j} \left\{ 1 - \Psi_6 \frac{(1 + A_2 O_j) \epsilon_r}{A_r \epsilon_2} \right\} \end{aligned} \quad (\text{F.1})$$

where $\Psi_6 = \frac{\delta_r}{x_r(t_1^1)}$. We have already established that an upper bound for the term $x_j(t_1^1)$ in expression (F.1) is equal to $-p_5 O_{\max}$ (see Appendix E). Hence, we can write

$$\begin{aligned} x_j(t_1^1 + \Delta t_{r1}) &< -p_5 O_{\max} \Psi_6 \frac{(1 + A_2 O_j) \epsilon_r}{A_r \epsilon_2} \\ &+ \frac{O_j}{1 + A_2 O_j} \left\{ 1 - \Psi_6 \frac{(1 + A_2 O_j) \epsilon_r}{A_r \epsilon_2} \right\}. \end{aligned} \quad (\text{F.2})$$

An upper bound for the right hand side of inequality (F.2) can be found if we substitute Ψ_6 with one of its lower bounds, and the O_j 's with O_{\max} . A lower bound on Ψ_6 is equal to δ_r . As a result, $x_j(t_1^1 + \Delta t_{r1}) < -p_5 O_{\max} p_8 + (1 - p_8) O_{\max} (1 + A_2 O_{\max})^{-1}$, where p_5 and p_8 are defined in Table V. Obviously, ART1 design constraint #4 is satisfied in the second competition cycle if the AART1-NN parameters are chosen according to CON15 in Table III.

ACKNOWLEDGMENT

The authors would like to thank the members of the BSP Group for their helpful discussions and suggestions.

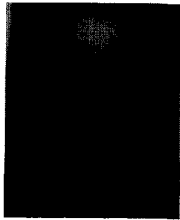
REFERENCES

- [1] G. A. Carpenter and S. Grossberg, "A massively parallel architecture for a self-organizing neural pattern recognition machine," *Computer Vision, Graphics, and Image Processing*, vol. 37, pp. 54-115, 1987.
- [2] M. W. Hirsch, "Convergent activation dynamics in continuous time networks," *Neural Net.*, vol. 2, no. 5 pp. 331-349, 1989.
- [3] S. N. Rasband, *Chaotic Dynamics of Nonlinear Systems*. New York: Wiley, 1990.
- [4] D. Ruelle, *Elements of Differentiable Dynamics and Bifurcation Theory*. San Diego, CA: Academic Press, 1989.
- [5] B. Kosko, *Neural Networks and Fuzzy Systems: A Dynamical Systems Approach to Machine Intelligence*. Englewood Cliffs, NJ: Prentice Hall, 1992.
- [6] M. W. Hirsch and S. Smale, *Differential Equations, Dynamical Systems, and Linear Algebra*. San Diego, CA: Academic Press, 1974.
- [7] C. Abdallah, G. L. Heileman, J. W. Howse, IV, and M. Georgiopoulos, "Dynamical neural networks as gradient systems," Tech. Rep. EECE, Univ. New Mexico, pp. 92-100, Sept. 1992.
- [8] J. J. Liou, C. S. Ho, M. Georgiopoulos, G. L. Heileman, and C. Christodoulou, "Design and simulation of adaptive resonance theory (ART) neural networks," in *SPIE Conf. Proc.*, Orlando, FL, 1993.
- [9] C. S. Ho, J. J. Liou, M. Georgiopoulos, G. L. Heileman, and C. Christodoulou, "Analog circuit design and implementation of an adaptive resonance theory (ART) neural network architecture," *Int. J. Elect.*, vol. 76, no. 2, pp. 271-291, 1994.
- [10] F. J. Pineda, "Dynamics and architecture for neural computation," *J. Complexity*, vol. 4, pp. 216-245, 1988.
- [11] R. J. Williams and D. Zipser, "A learning algorithm for continually running fully recurrent neural networks," *Neural Computation*, vol. 1, no. 2, pp. 270-280, 1989.
- [12] K. S. Narendra and K. Parthasarathy, "Gradient methods for the optimization of dynamical systems containing neural networks," *IEEE Trans. Neural Net.*, vol. 2, pp. 252-262, 1991.
- [13] G. A. Carpenter and S. Grossberg, "ART 2: Self-organization of stable category recognition codes for analog input patterns," *Appl. Optics*, vol. 26, no. 23, pp. 4919-4930, 1987.
- [14] ———, "ART 3: Hierarchical search using chemical transmitters in self-organizing pattern recognition architectures," *Neural Net.*, vol. 3, no. 2, pp. 129-152, 1990.
- [15] M. Georgiopoulos, G. L. Heileman, and J. Huang, "Properties of learning related to pattern diversity in ART1," *Neural Net.*, vol. 4, no. 6, pp. 751-757, 1991.
- [16] ———, "The N-N-conjecture in ART1," *Neural Net.*, vol. 5, no. 5, pp. 745-753, 1992.
- [17] G. A. Carpenter, S. Grossberg, and D. B. Rosen, "ART 2-A: An adaptive resonance algorithm for rapid category learning and recognition," *Neural Net.*, vol. 4, no. 4, pp. 493-504, 1991.

Gregory L. Heileman (S'89-M'89) received the B.S. degree from Wake Forest University in 1982, the M.S. degree in biomedical engineering and mathematics from the University of North Carolina-Chapel Hill in 1986, and the Ph.D. degree in computer engineering from the University of Central Florida in 1989.

He is currently an Assistant Professor in the Electrical and Computer Engineering Department at the University of New Mexico, Albuquerque, NM. His research interests include neural networks, computational learning theory, parallel computing, and pattern recognition.

Dr. Heileman is a member of the IEEE Computer Society, the Association for Computing Machinery, and the International Neural Network Society.



Michael Georgiopoulos (S'84–M'86) received the Diploma in electrical engineering from the National Technical University of Athens, Greece in 1981, and the M.Sc. and Ph.D. degrees in electrical engineering from the University of Connecticut, Storrs, in 1983 and 1986, respectively.

In January 1987, he joined the University of Central Florida, Orlando, where he is presently and Associate Professor in the Department of Electrical Engineering. His current research interests are in the areas of neural networks and spread spectrum communications.

Dr. Georgiopoulos is a member of the Technical Chamber of Greece and the International Neural Network Society.



Chaouki Abdallah (S'87–M'88) received the B.E. degree in electrical engineering in 1981 from Youngstown State University, OH, the M.S. degree in 1982 and the Ph.D. degree in electrical engineering in 1988 from Georgia Tech, Atlanta, GA.

Between 1983 and 1985 he was with SAWTEK Inc., Orlando, FL. In September of 1988 he joined the Department of Electrical And Computer Engineering at the University of New Mexico, Albuquerque, NM where he is presently an

Associate Professor. His research interests are in the areas of dynamic neural networks, nonlinear and robust control, and robotics. He is also a co-editor of the book *Robot Control: Dynamics, Motion Planning, and Analysis*, (IEEE) and co-author of a book titled *Robot Control* (Macmillan, 1993).

Dr. Abdallah was exhibit chairman of the 1990 International Conference on Acoustics, Speech, and Signal Processing (ICASSP), in Albuquerque, NM. He is a member of Sigma Xi and Tau Beta Pi.